The following is a version of record of the journal paper: An, L. S., Alinejad, N., Kim, S., & Jung, S. (2023). Experimental study on wind characteristics and prediction of mean wind profile over complex heterogeneous terrain. *Building and Environment*, *243*, 110719.

EXPERIMENTAL STUDY ON WIND CHARACTERISTICS AND PREDICTION OF MEAN WIND PROFILE OVER COMPLEX HETEROGENEOUS TERRAIN

Lee-Sak An[1], Nasrollah Alinejad[2], Sejin Kim[3], and Sungmoon Jung[4]*

Abstract

This study investigates the impact of complex heterogeneous terrain on mean wind speed and turbulence intensity, highlighting the significance of terrain configuration in the wind loading on buildings and airflow over urban areas. Extensive wind tunnel tests were conducted for 60 different roughness configurations, obtained by processing aerial images across the United States. The study makes two main contributions. First, a model was proposed to predict mean wind profiles, using the morphological information of complex heterogeneous terrain. The Deaves and Harris model was utilized along with a novel algorithm for the automatic characterization of roughness transitions. The proposed model exhibited less than 2 % average prediction error compared to the measured wind speed. Second, the study investigated the impact of terrain complexity on near-surface wind characteristics. By comparing the experimental results with those obtained from a homogeneous terrain with a similar roughness length, we quantified the potential errors that may arise when assuming a homogeneous terrain for wind speed assessment. It was observed that increasing variability in roughness length led to a

[1] Postdoctoral Scholar, Department of Civil and Environmental Engineering, FAMU-FSU College of Engineering, 2035 E Paul Dirac Dr, Tallahassee, Florida 32310, United States. Email: lan@eng.famu.fsu.edu

[2] Ph.D. candidate, Department of Civil and Environmental Engineering, FAMU-FSU College of Engineering, 2035 E Paul Dirac Dr, Tallahassee, Florida 32310, United States. Email: na19j@fsu.edu

[3] Postdoctoral Scholar, Department of Civil and Environmental Engineering, University of Michigan, 2350 Hayward ST GG Brown 1267A, Ann Arbor, Michigan 48109, United States. Email: sejinki@umich.edu

[4] Professor, Department of Civil and Environmental Engineering, FAMU-FSU College of Engineering, 2035 E Paul Dirac Dr, Tallahassee, Florida 32310, United States. Email: sjung@eng.famu.fsu.edu (corresponding author)

decrease in mean wind speed and an increase in turbulence intensity. The influence of terrain complexity, however, was found to be secondary compared to roughness length. Consequently, the relationships between terrain complexity and wind characteristics were quantified, and a simplified model was proposed.

Keywords

Complex heterogeneous terrain, Wind tunnel testing, Wind characteristics, Deaves and Harris model, Roughness change, Terraformer

1. Introduction

The terrain configuration plays a crucial role in influencing wind loading on buildings or air flow over urban areas. The roughness of the terrain introduces uncertainties in near-surface wind characteristics, leading to numerous research efforts investigating the impact of terrain heterogeneity on wind patterns and wind loads.

Field measurements have provided invaluable ground truth data, predominantly focusing on moderately homogeneous terrains [1-4]. However, these measurements cannot meet the data demands in areas with sparse sites, such as complex morphologic regions. Wind tunnel testing offers the advantage of controlling test parameters. Counihan [5, 6] employed a wind tunnel system consisting of a barrier, vortex generators, and surface roughness to stimulate boundary layer growth. Cook [7, 8] used a grid, a barrier, and surface roughness to simulate the lower portion of the neutral atmospheric boundary layer (ABL), commonly known as the atmospheric surface layer (ASL). Irwin [9] proposed a formula for the design of spires for use in simulating the boundary layer. These pioneers addressed fundamental issues in wind tunnel testing, such as model scale and wind tunnel size. Kozmar [10, 11] investigated truncated vortex generators for wind tunnel simulation of boundary layer flow. Other notable studies have examined the effects of upstream urban areas [12] and suburban regions [13] on wind characteristics.

The roughness length is commonly used in ASL modeling to simulate the underlying surface's influence on turbulent mixing. An effective roughness value for the entire area has been found to be sufficient in areas with moderately homogeneous terrains and smaller-scale inhomogeneity (such as vegetation patches and built structures) [14, 15]. However, terrains in the real world are often complex and have abrupt changes in surface roughness, such as transitions from water bodies to land or grasslands to agricultural land. Wind flow over such surface roughness transitions is sensitive to surface properties. The applicability of the effective roughness length for such complex heterogeneous terrains remains unknown. Prior researchers were also aware that roughness changes significantly impact boundary layer estimation [16, 17]. Since the wind tunnel modeling of wind pressure on buildings can be severely biased if incorrect upwind roughness is used, it is necessary to quantify the impact of terrain complexity that occurs in the real world. For terrain transitions, such as rough-to-smooth (R-S) or smooth-to-rough (S-R), Panofsky and Townsend [18] proposed a theory assuming a linear variation of friction velocity from the ground to the internal boundary layer top. This theory was later generalized by Townsend [19]. Ghaisas [20] proposed a predictive model for the velocity profile behind a surface roughness transition based on Townsend's model. The Deaves and Harris model [21, 22] was formulated to numerically solve the equations of motion for two-dimensional mean wind flows over roughness changes. The model has significantly influenced subsequent research [23-25] as well as standards [26-28]. Additionally, various numerical and experimental studies have conducted in-depth investigations on wind profiles over R-S transitions [29-31] and S-R transitions [31-33].

Despite these previous studies, significant knowledge gaps remain regarding the influence of the complex heterogeneous terrain on near-surface wind profiles. The major limitation is the setup of realistic roughness elements. As a result, previous experimental studies have primarily investigated simple terrain transitions [25, 34, 35] or a limited number of complex heterogeneous terrains [12, 36, 37]. Consequently, a more comprehensive dataset from wind tunnel testing is needed, encompassing a diverse range of surface morphologies to accurately evaluate the impact of terrain complexity on near-surface wind profiles.

This study presented an experimental investigation into the influence of complex heterogeneous terrain on wind characteristics, particularly focusing on the near-surface wind profile (~30 m), where local terrain has a pronounced effect on wind characteristics. The roughness elements in the wind tunnel were carefully configured based on National Land Cover Database and aerial images obtained from 60 distinct sites across the United States. The study had two main contributions. First, an approach to predict the mean wind profile over complex heterogeneous terrain was developed, leveraging the morphological information of the terrain. This approach combined the Deaves and Harris model with a new detection algorithm to characterize roughness transitions automatically without subjective decisions. To validate the proposed approach, wind speeds from wind tunnel testing were compared against the predicted mean wind profiles. Second, how terrain complexity impacts wind characteristics in the atmospheric surface layer was examined. The degree of wind profile change according to the level of inhomogeneity was confirmed by comparing it with the experimental results on homogeneous terrain. Wind characteristics, including mean wind speed and turbulence intensity, were investigated to observe changes associated with variations in terrain complexity. Differences in wind characteristics that could occur when complex heterogeneous terrain was simplified to equivalent homogeneous terrain were quantified. Consequently, the relationship between the morphologic complexity of heterogeneous terrain and wind characteristics was quantified.

2. Test Setup

2.1. Wind Tunnel and Terraformer

The experiments were conducted in the boundary layer wind tunnel (BLWT) located at the University of Florida [38]. Fig. 1 presents a schematic plan of the tunnel, which is an open circuit tunnel with dimensions of 6 m (width) × 3 m (height) × 38 m (length). The tunnel inlet contains eight vane axial fans, each powered by a 56 kW electric motor. The flow generated by the fans is conditioned by honeycombs situated approximately 3 m downwind from the fan bank.

This facility is equipped with a state-of-the-art, fully-automated terrain simulator called the "Terraformer." This advanced technology enables rapid and precise terrain simulation, addressing the time-consuming and labor-intensive challenges associated with wind tunnel testing [39]. The Terraformer consists of an 18 × 62 computer-controlled array of roughness blocks in a staggered configuration, covering a fetch size of 6.1 m × 18.6 m. Each roughness element is equipped with an actuator, allowing for independent height adjustments. The elements have a plan dimension of 100 mm × 50 mm and adjustable heights ranging from 0 to 160 mm. The element height is controlled through LabVIEW software, and the reconfiguration of all 1,116 elements generally takes less than 60 seconds. As a result, the Terraformer can efficiently simulate an extensive series of homogeneous and heterogeneous upwind terrains. Additionally, a turntable at the end of the upwind fetch enables the simulation of wind effects on structures at various flow incidence angles.

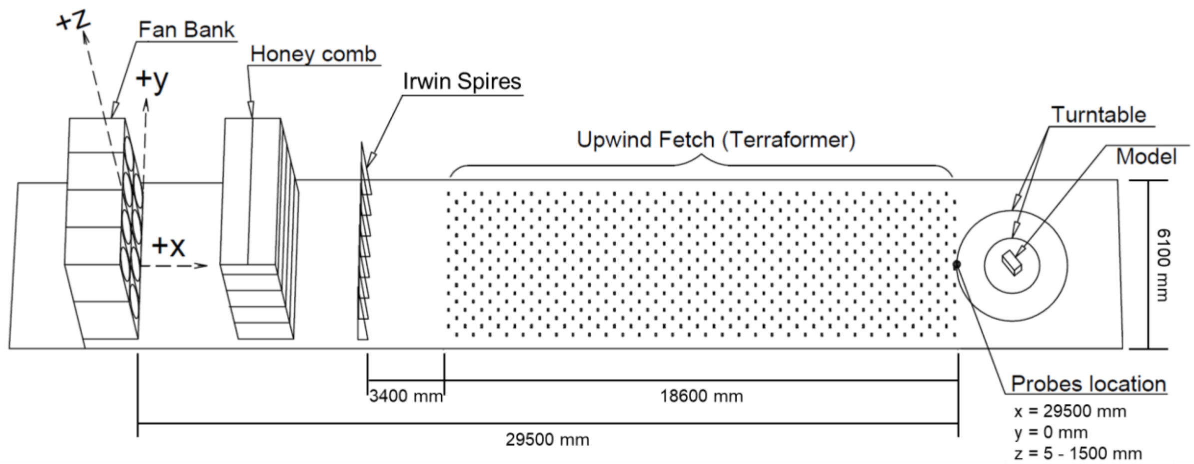

Fig. 1. Schematic diagram of the wind tunnel at the University of Florida.

The wind speed profile was measured using three Turbulent Flow Instrumentation Cobra Probes placed at the center of the Terraformer. These probes accurately captured the three velocity components at a sample rate of 1,250 Hz. Measurements were taken at 36 heights, ranging from 5 mm to 1,500 mm above the ground. Additionally, further wind profile measurements were obtained at ±300 mm and ±600 mm along the y-axis (crosswind direction) in specific test cases.

This study utilized two distinct length scales, 1:50 and 1:100. As Stathopoulos [40] summarized, simulating only the lower region of the atmospheric surface layer with larger model scales (such as 1:50 to 1:100) is an effective approach for addressing the length scale problem encountered in wind tunnel testing. More extensive wind tunnel testing results were obtained by conducting tests at two different scales for the complex heterogeneous terrains. We focused on examining the near-surface wind profile (~30 m), where local terrain roughness significantly impacts wind characteristics. It is widely acknowledged that the wind profile in the higher boundary layer range is less affected by terrain roughness changes [25]. For 1:50 and 1:100 scales, Terraformer generates terrains of 305 m × 930 m and 610 m × 1,860 m, respectively. The maximum full-scale heights considered for wind profile measurements were 75m and 150m for the 1:50 and 1:100 scales, respectively. The test duration for each scale equated to 10 minutes of full-scale measurement, with 45 seconds for both 1:50 and 1:100 scales. The wind speeds were adjusted to correspond with the respective scales, resulting in speed scales of 3.75 ($\frac{V_{full}}{V_{test}} = \frac{50}{600} / \frac{1}{45}$) for the 1:50 scale and 7.5 ($\frac{V_{full}}{V_{test}} = \frac{100}{600} / \frac{1}{45}$) for the 1:100 scale.

Note that pressure data were collected using a 1:50 scale model representing a low-rise building and a 1:100 scale model representing a mid-rise building. However, the detailed analysis and discussion of wind pressure on buildings were beyond the scope of this research. Therefore, this study did not include discussions on wind pressure on buildings.

2.2. Selection of Heterogeneous Terrains

Heterogeneous terrain configurations in the real world were gathered for wind tunnel testing. The primary source of information for this purpose was the National Land Cover Database (NLCD) [41], provided by the U.S. Geological Survey. The NLCD uses Landsat data to document various land cover types throughout the U.S. A total of 529 sites in 32 U.S. states, prone to hurricanes, were chosen for the study.

Each site image obtained from the NLCD dataset had dimensions of 3,840 m × 3,840 m. To ensure comprehensive coverage, each image was divided into four smaller images facing north, south, west, and east, measuring 1,860 m × 540 m each. This division resulted in a total of 2,116 images for analysis. The NLCD dataset provided land coverage details for each pixel in the image. Utilizing the corresponding local roughness length (z_0^{local}) values from Table 1 for specific land coverage types, each pixel in the image was assigned the relevant z_0^{local} value. In the wind tunnel, these z_0^{local} values were then associated with the appropriate block height using the improved Lettau relationship proposed by Macdonald et al. [42], which can also be found in Table 1.

To choose representative terrains with unique stochastic properties of z_0^{local} without overlap, the mean $\mu(z_0^{local})$ and standard deviation $\sigma(z_0^{local})$ of each image were plotted in a two-dimensional (2D) space, as illustrated in Fig. 2. A 2D k-means algorithm [43], a widely used clustering method that minimizes the average squared distance between points in the same cluster, was applied to the 2D space. The k-means algorithm identified and classified 50 distinct clusters. The representative sites for each cluster, known as cluster centroids, were then selected. In Fig. 2, the 50 chosen sites are represented by cross marks.

Table 1. Land coverage classification in NLCD images. The z_0 range is based on Wieringa [15], Wang and Stathopoulos [25], Davenport [44], Vihma and Savijärvi [45], and He et al. [46].

Land cover	z_0^{Local} (full-scale, m)	Block height (test-scale, m)	
		1:50	1:100
Open Water, Perennial Ice, Snow	0.0003	0.0060	0.0050
Woody Wetlands, Emergent Herbaceous Wetland	0.0025	0.0100	0.0085
Barren Land	0.0055	0.0125	0.0105
Dwarf Scrub, Shrub Scrub	0.0105	0.0160	0.0125
Pasture, Hay	0.0155	0.0180	0.0145
Grassland, Herbaceous, Cultivated Corps	0.0205	0.0200	0.0155
Low-rise building	0.5	0.0770	0.0545
Mid- to high-rise	1	0.1110	0.0770
Deciduous Forest, Evergreen Forest, Mixed Forest	1.65	0.1480	0.1000

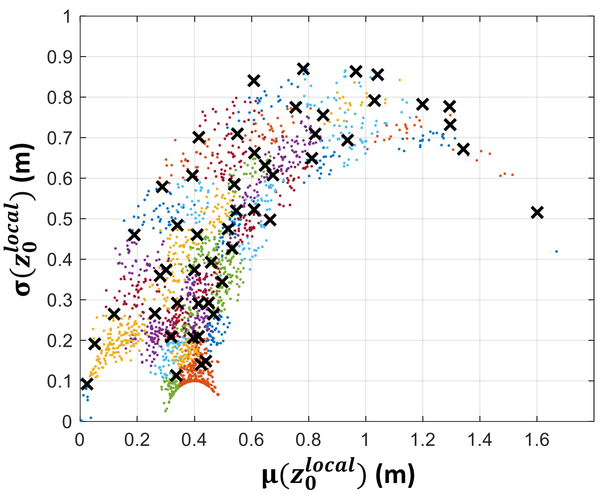

Fig. 2. 2D clustering results using $\mu(z_0^{local})$ and $\sigma(z_0^{local})$ for each site. Dots represent the investigated sites, while cross marks indicate the selected sites. The clusters are color-coded, with a total of 50 colors.

In addition, ten manual selections were made from seven cities that had experienced significant hurricane events in recent decades. These cities are Port Sulphur (LA), Frisco (NC), Satellite Beach (FL), Bonita Springs (FL), Rockport (TX), Port Lavaca (TX), and Somers Point (NJ). A total of 60 sites were chosen for wind tunnel testing. Appendix A lists the coordinates for each site. Fig. 3 displays examples of the selected sites and their respective block height maps. Fig. 4 illustrates the simulated terrain morphology created by the Terraformer for site 8.

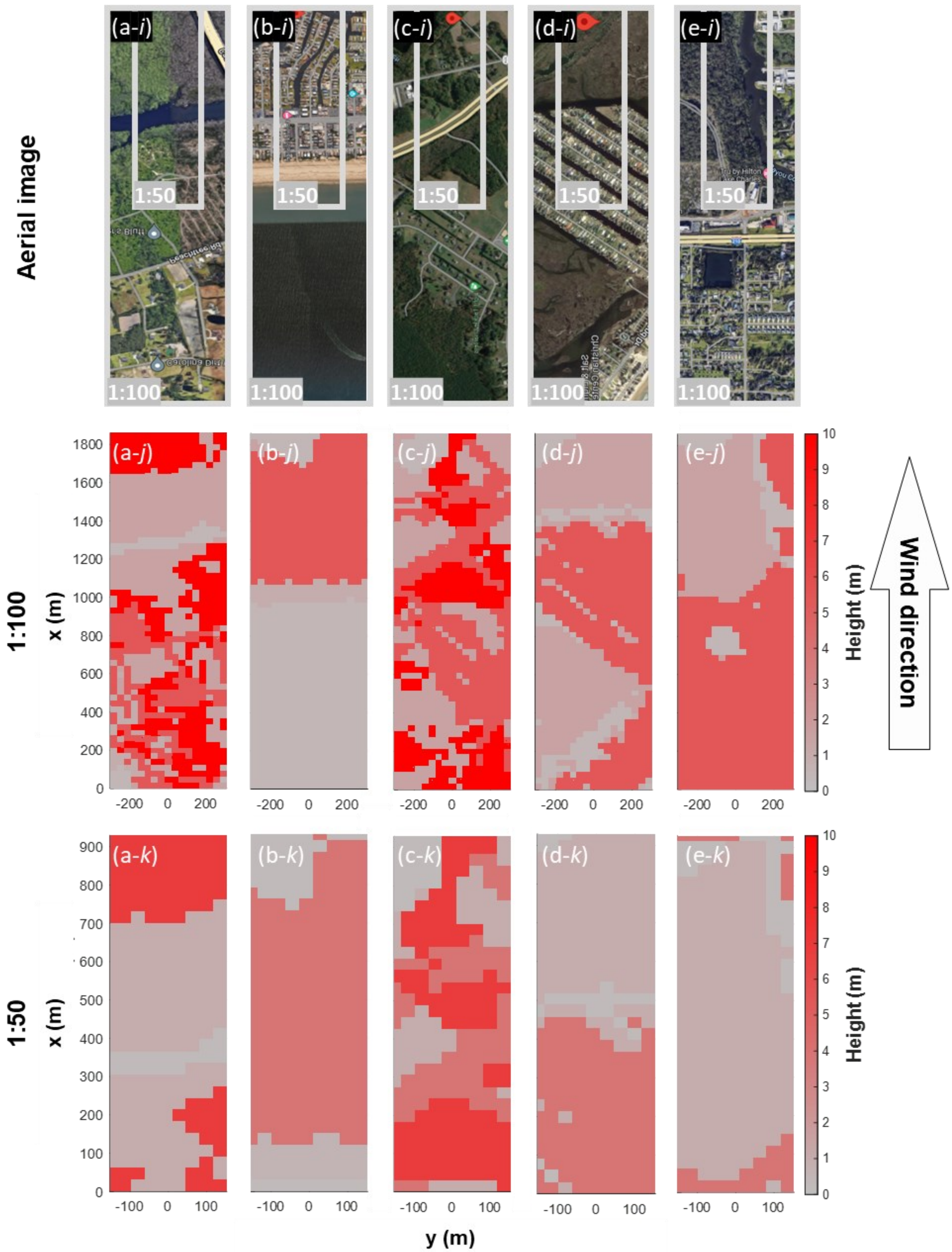

Fig. 3. Examples of five complex heterogeneous sites: (a) Site 8; (b) Site 13; (c) Site 31; (d) Site 34; and (e) Site 45. (i) Aerial image; (j) Corresponding block height maps in a 1:100 scale; and (k) 1:50 scale.

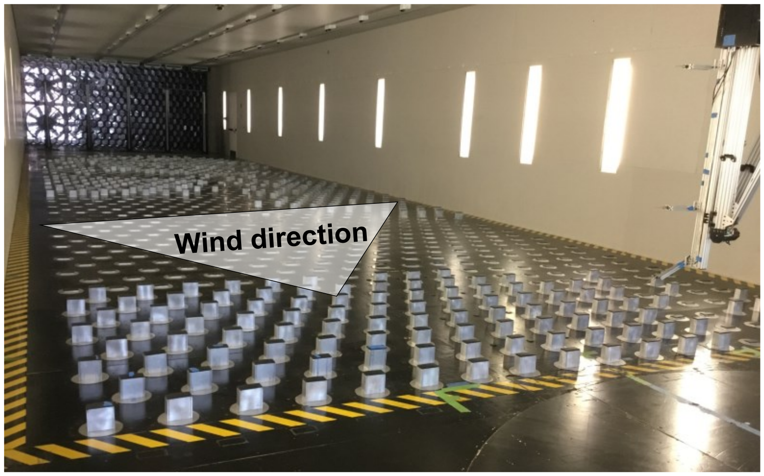

Fig. 4. Implementation of complex heterogeneous terrain in Terraformer, specifically Site 8, in a 1:100 scale based on Fig. 3 (a-j).

3. Mean Wind Profile Prediction

This section presents a method for predicting the mean wind speed across complex heterogeneous terrain by using terrain morphology information. It is crucial to accurately capture the influence of roughness changes when predicting wind profiles for such terrain. To tackle this issue, the Deaves and Harris (DH) model was employed, which is a widely used model for assessing wind profiles on terrains with varying roughness. In addition, a mathematical change detection algorithm was incorporated to automatically and quantitatively identify changes in roughness.

3.1. Deaves and Harris model

Fig. 5 illustrates the conceptualization of the mean wind profile at location x_n following a roughness change. In the DH model, a transition region lies between a new internal boundary layer and the original outer boundary layer. To adapt the DH model to the complex heterogeneous terrain involving intricate arrangements of various roughness elements, the model requires a careful assessment of roughness changes. The following sections provide a detailed explanation of how the DH model was adapted to predict the mean wind speed within the context of complex heterogeneous terrain.

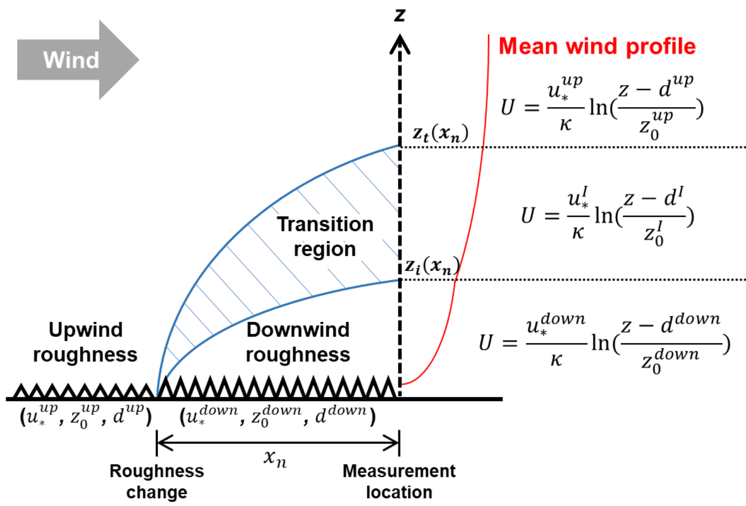

Fig. 5. Conceptual illustration of the mean wind profile over a roughness change.

First, mean wind profiles in the equilibrium state were determined for the upwind and downwind regions. The surface layer, primarily influenced by surface friction [47], is the main focus of this study. Therefore, the derivation of the mean wind profile utilized the logarithmic wind law [48]. The logarithmic wind law, known for its widespread acceptance and accurate representation of the theoretical mean wind speed in the lower portion of the ABL [49], is described by Eq. (1):

$$U(z) = \frac{u_*}{\kappa} \ln\left(\frac{z-d}{z_0}\right) \tag{1}$$

where $U(z)$ represents the mean along-wind speed at height z, κ is von Karman's constant (= 0.40), u_* is the friction velocity, z_0 stands for the aerodynamic roughness length, and d represents the zero-plane displacement. This equation holds when the surface is aerodynamically fully-rough—i.e., the surface-roughness Reynolds number $Re_* = u_* z_0/\nu > 2.5$ [50], where ν is the kinematic viscosity of air. Among all wind tunnel testing results in this study, only four homogeneous cases ($H \leq 0.9$ cm) showed the Re_* values lower than 2.5. Collectively, the parameters, u_*, z_0, and d, are referred to as aerodynamic roughness parameters (ARPs). The methodology for obtaining ARPs on complex heterogeneous terrain, specifically utilizing terrain morphology information such as block height information, will be explained in detail in Section 3.2.

In the subsequent stage, a modified wind profile that incorporates roughness changes was developed. These changes encompassed two types of transitions: rough-to-smooth (R-S) and smooth-to-rough (S-R). In the R-S transition, the upwind terrain has a higher z_0 than the downwind terrain, while the S-R transition involves the opposite scenario. To account for the roughness change, a transition region was introduced between the new internal boundary layer and the original outer boundary layer. This transition region was defined by the inner layer depth (z_i) and the outer layer depth or transition region height (z_t). Below z_i, the flow reaches a local equilibrium with the downwind surface, while above z_t, the flow remains unaffected by the upwind roughness. The values of z_i for the R-S and S-R transitions are given by Eqs. (2) and (3) proposed by Deaves [22]:

$$z_i(x_n) = 0.07x_n\sqrt{\frac{z_0^{down}}{z_0^{up}}} \tag{2}$$

$$z_i(x_n) = 0.36x_n^{0.75}\left(z_0^{down}\right)^{0.25} \tag{3}$$

Here, z_0^{up} and z_0^{down} represent the roughness lengths of the upwind and downwind regions, respectively, while x_n denotes the downwind fetch length. These equations capture the gradual growth of the internal boundary layer as the wind flows through the roughness change.

The transition region height, z_t, remains unaffected by the direction of the roughness change but is influenced by z_{0+}, which corresponds to the larger of the z_0^{up} and z_0^{down}, as shown in Eq. (4) [22]:

$$z_t(x_n) = 10x_n^{0.6}z_{0+}^{0.4} \quad (4)$$

The non-equilibrium flow within the transition region, from z_i and z_t, exhibits distinct characteristics compared to the original and new boundary layers. It was postulated that a pair of interpolation parameters could describe the profiles in this region (u_*^I, z_0^I) that vary monotonically across the transition region. Detailed formulations for these interpolation parameters can be found in Deaves [22]. It is worth noting that if there are no roughness changes in the terrain, the mean wind speed profile can still be predicted using Eq. (1) alone.

3.2. Roughness Change Detection

A novel approach was proposed to detect and characterize roughness changes in complex heterogeneous terrain. While identifying roughness change locations is relatively straightforward in simple heterogeneous terrains, it becomes challenging in the presence of complex morphology, which can impede the application of the DH model. The primary objective of the proposed approach was to eliminate subjectivity and accurately determine the presence and location of roughness changes, thus enabling its applicability across various terrain types.

First, the block height (H) maps of the terrains were transformed into corresponding roughness length (z_0) maps. The relationship between H and z_0 was established beforehand through wind tunnel testing conducted under uniform block height conditions. Detailed data from the preliminary testing can be found in Appendix B. If the coefficient of variation of z_0 (COV_{z_0})

within the maps fell below a predefined threshold (T_{COV}), the terrain was considered homogeneous without any roughness transitions. However, if the COV_{z_0} exceeded T_{COV}, an optimal detection algorithm based on linear computational cost [51] was employed to identify abrupt changes in z_0 along the wind direction (x-axis), as described by Eq. (5).

$$\sum_i C(\boldsymbol{A}_i) + T_c < C(\boldsymbol{A}) \tag{5}$$

where $\boldsymbol{A}$ is a vector of data containing change points that can be split into multiple segments $\boldsymbol{A}_i$, T_c (m^2) represent a threshold for abrupt change. The cost function, C, is defined by Eq. (6):

$$C(\boldsymbol{X}) = N(\boldsymbol{X}) \times Var(\boldsymbol{X}) \tag{6}$$

Here, $N(\boldsymbol{X})$ and $Var(\boldsymbol{X})$ represent the number of elements and the variance of vector X, respectively. If a change point was detected, the terrain was classified as an equivalent heterogeneous terrain with roughness changes. Conversely, if no change point was detected, the terrain was considered an equivalent homogeneous terrain.

Following the roughness change detection, the terrain was divided into upwind and downwind fetches based on the identified change point. This division naturally determined the length of the downstream fetch (x_n in Fig. 5). Subsequently, the effective roughness length ($z_{0,eff}$) for each fetch was calculated using a grid-squared average-based approach, utilizing the z_0 maps [45, 52]. The approach relied on the linear approximation of the Rossby number similarity theory and derived the following formula [45]:

$$\ln\left(z_{0,eff}\right) = \langle \ln\,(z_0) \rangle + a\sigma^2_{ln(z_0)} \tag{7}$$

Here, a represents the Rossby value, typically set to 0.09, and $\sigma^2_{ln(z_0)}$ indicates the variance within the area. The $\langle\ \rangle$ notation represents the area-weighted logarithmic average operation. If the terrain is equivalent homogeneous, a single $z_{0,eff}$ value is calculated for the entire fetch. In Eqs. (1)-(4), z_0 is replaced by $z_{0,eff}$.

The other aerodynamic roughness parameters (d and u_*) are also determined based on their relationships with $z_{0,eff}$ and the ARPs, as described in Fig. B. 2 of Appendix B. Additionally, the z_i, z_t, and interpolation parameters (u_*^I, z_0^I) are calculated using x_n and $z_{0,eff}$. Finally, the mean wind profiles are predicted using the DH model, taking into account the presence and location of roughness changes. The entire process, from the block height map to the prediction of mean wind profiles, is summarized in Fig. 6.

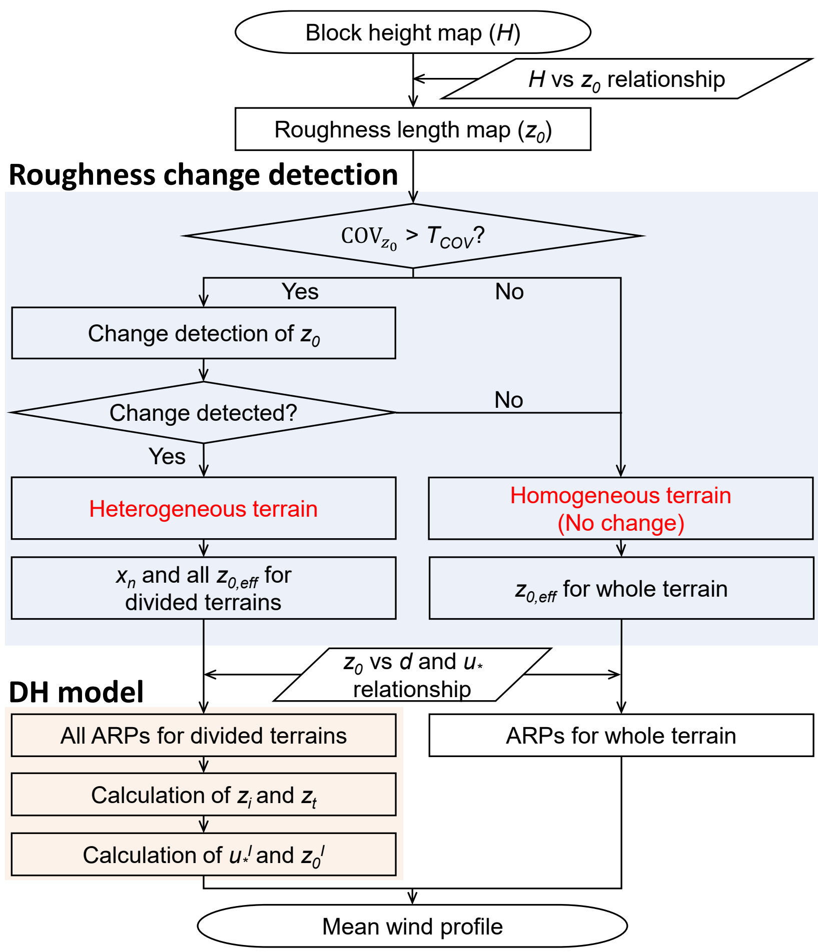

Fig. 6. Proposed process for predicting mean wind profile in complex heterogeneous terrain.

The thresholds T_{COV} and T_c significantly impact the prediction performance of the proposed process. If T_{COV} is set too high, terrains with moderate heterogeneity may be mistakenly classified as homogeneous. Similarly, increasing T_c requires a more pronounced morphological change to be detected as a roughness change, resulting in more cases being classified as equivalent homogeneous terrain. Hence, a parametric study was conducted to optimize T_{COV} and T_c, aiming to enhance the prediction performance of the proposed process. The performance evaluation relied on the prediction error ($\varepsilon_U(z)$), which measures the disparity between the measured and predicted mean wind speeds at height z, as expressed in Eq. (8).

$$\varepsilon_U(z) = \frac{U_{Test}(z) - U_{Pred}(z)}{U_{Test}(z)} \times 100\ \% \tag{8}$$

Here, U_{Test} and U_{Pred} represent the measured and predicted mean wind speeds for complex heterogeneous terrains, respectively. Fig. 7 provides an illustration of the mean, standard deviation, and maximum absolute values of $\varepsilon_U(10\ m)$ as T_c varies on a 1:50 scale. The results show that the mean prediction error exhibits satisfactory accuracy across the entire range of T_c values, with magnitudes consistently below 3%. However, for T_c values exceeding 0.8 m^2, the maximum absolute value of $\varepsilon_U(10\ m)$ decreases rapidly to less than 20%. A similar study was conducted for T_{COV}, and the optimal values determined were 0.25 for T_{COV} and 0.8 m^2 for T_c.

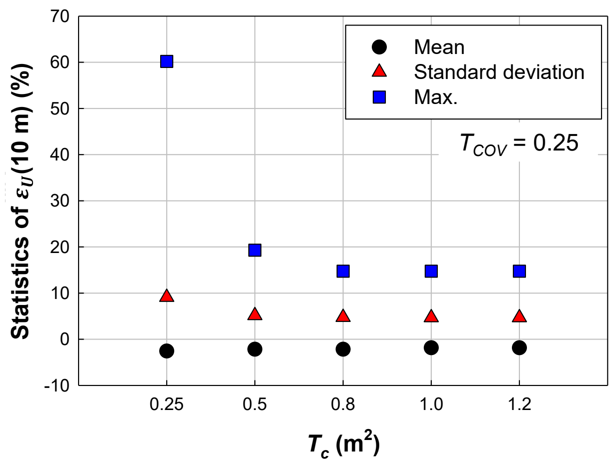

Fig. 7. Statistical characteristics of $\varepsilon_U(10\ m)$ as T_c changes at a 1:50 scale.

3.3. Example Predictions Using the Proposed Model

Fig. 8 showcases the mean wind speed prediction results for three representative sites: 8, 31, and 34. The figures include the block height maps (i), the outcomes of roughness change detection (j), and a comparison between the predicted and measured wind profiles (k).

Site 8 (Fig. 8 (a)) shows a noticeable change in block height around 700 m along the x-axis. The roughness change detection algorithm accurately identified this location, classifying the site as an equivalent heterogeneous terrain with an S-R change, as shown in Fig. 8 (a-j). $z_{0,eff}$ for the upwind and downwind terrains were determined to be 0.02 m and 0.59 m, respectively. In such a change of roughness length from smooth to rough, the surface drag increases, and consequently, the near-wall flow decelerates. With the consideration of the roughness change, the predicted mean wind profiles showed good agreement with the measured wind profiles, as depicted in Fig. 8 (a-k). The $\varepsilon_U(10\ m)$ was 0.3% under the assumption of equivalent heterogeneity. In comparison, when the roughness change was not considered (equivalent homogeneous assumption), the $\varepsilon_U(10\ m)$ increased significantly to 23.7%.

For site 31 (Fig. 8 (b)), both the wind and crosswind directions exhibited high complexity, making it visually challenging to identify a roughness change location. The roughness change detection algorithm classified this terrain as an equivalent homogeneous terrain with $z_{0,eff}$ of 0.21 m. The $\varepsilon_U(10\ m)$ was determined to be 10.5%.

For site 34 (Fig. 8 (c)), an R-S change was identified at approximately 450 m. The upwind and downwind terrains had $z_{0,eff}$ of 0.21 m and 0.01 m, respectively. In such a roughness change from rough to smooth, the surface drag decreases, and the near-wall flow accelerates. Considering the roughness change, enhanced prediction performance was observed. The $\varepsilon_U(10\ m)$ was 4.4% with the consideration of the roughness change and 7.1% without it.

The proposed model accurately predicted mean wind speed profiles, thanks to the implemented roughness change detection algorithm. Not accounting for roughness changes when estimating the near-surface mean wind profile for complex heterogeneous terrains can lead to significant errors. However, as shown in Fig. 8 (b), the complexity of terrain morphology can impact the prediction performance, highlighting the need to further explore the variations in performance based on the degree of terrain complexity. The current approach utilizing ARPs does not fully capture terrain irregularities, necessitating additional investigation into this aspect.

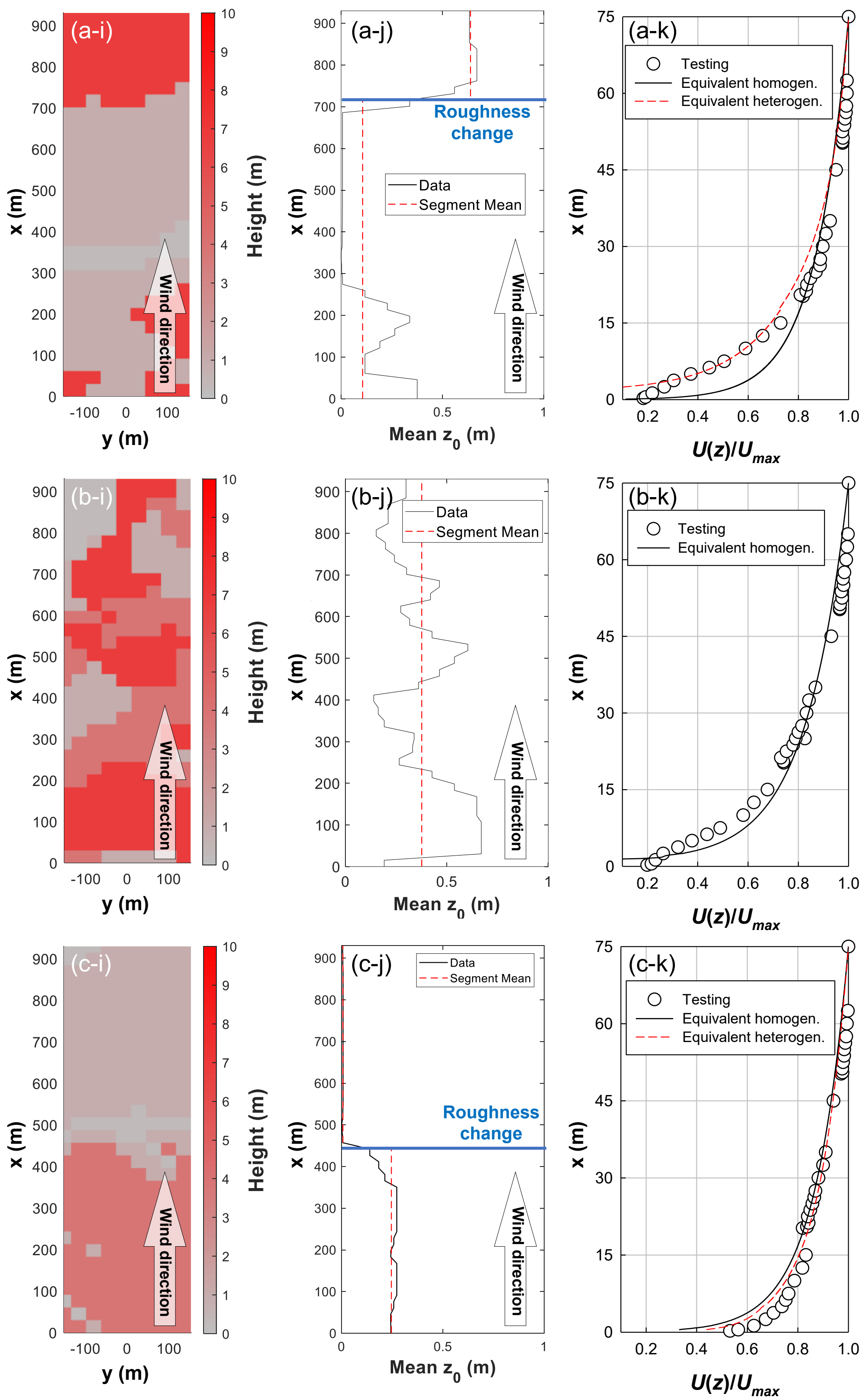

Fig. 8. Mean wind profile prediction for (a) site 8, (b) 31, and (b) 34 at a 1:50 scale: (i) Block height map; (j) Result of roughness change detection; and (k) Comparison of measured and predicted mean wind speed.

3.4. Prediction Performance

Fig. 9 depicts the scatter of $\varepsilon_U(10\ m)$ and $\varepsilon_U(30\ m)$ at 120 sites in relation to $\mathrm{COV}_{\ln(z_0)}$. ln(z_0) was chosen to represent exposure roughness due to the wide distribution of z_0 values spanning multiple orders of magnitude and the substantial impact of ln(z_0) on wind speed according to the logarithmic wind law. The results demonstrate a high prediction performance with mean values of -1.4 and -1.8, respectively. While the mean values of ε_U did not exhibit significant differences between the two heights, the standard deviation of $\varepsilon_U(30\ m)$ (3.5) showed a reduction of over 50% compared to that of $\varepsilon_U(10\ m)$ (7.4). This indicates that the influence of terrain complexity and wind speed variability relative to the theoretical mean wind speed is greater at lower heights within the surface layer.

The investigation further revealed that an increase in $\mathrm{COV}_{\ln(z_0)}$ had an adverse effect on the prediction performance, even when $z_{0,eff}$ values were similar. The negative sign of $\varepsilon_U(z)$ indicated that the measured wind speed was lower than the predicted value, suggesting that increased terrain complexity resulted in greater disruption of the wind flow, leading to a lower wind speed than the theoretical mean wind speed. This relative reduction in measured wind speed compared to the theoretical value was more prominent at lower $z_{0,eff}$ values. For instance, when $z_{0,eff}$ was below 0.1, an $\varepsilon_U(10\ m)$ of up to -20% was observed when the $\mathrm{COV}_{\ln(z_0)}$ reached approximately 0.7. Conversely, within the range of $0.3 < z_{0,eff} \leq 0.4$, $\varepsilon_U(10\ m)$ reached around -20% when the $\mathrm{COV}_{\ln(z_0)}$ exceeded 1.2.

The decrease in prediction performance can be attributed to the inherent limitations of existing wind speed profile models. These models rely on a limited number of parameters, primarily z_0, to account for the influence of terrain characteristics on the wind speed profile, which proves insufficient in adequately capturing the complexity of terrain morphology. Further studies can explore the introduction of new parameters related to terrain complexity, enabling the development of a model that maintains high accuracy across a wider range of $\mathrm{COV}_{\ln(z_0)}$ values.

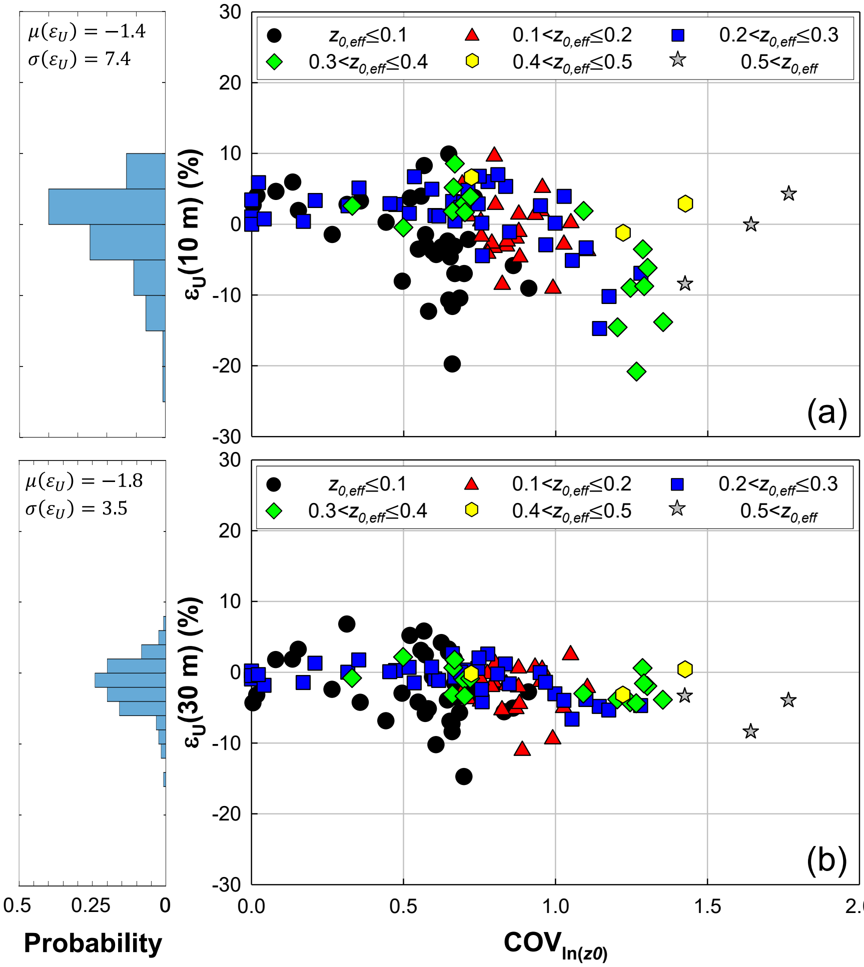

Fig. 9. Impact of $\mathrm{COV}_{\ln(z_0)}$ on the prediction error of mean wind speed between measured and predicted results ($z_{0,eff}$ unit: m): (a) 10 m height; and (b) 30 m height.

The prediction performance was also assessed for different positions along the *y*-axis, perpendicular to the prevailing flow. At sites 36 to 45, wind profiles were measured not only at the original measurement location (*y*=0 mm) but also at positions ±300 mm and ±600 mm along the *y*-axis. Among these sites, site 40 exhibited the most pronounced changes in near-surface wind flows, as depicted in Fig. 10. Evaluating the prediction performance revealed that the mean and standard deviation of $\varepsilon_U(10\ m)$ for the ten sites (comprising a total of 20 cases for both 1:50 and 1:100 scales) were below 5%. The maximum absolute value of $\varepsilon_U(10\ m)$ was approximately 13%. These findings demonstrate that the proposed process consistently delivered reasonable prediction performance across various locations within ±600 mm from the center of the *y*-axis in the testing scale.

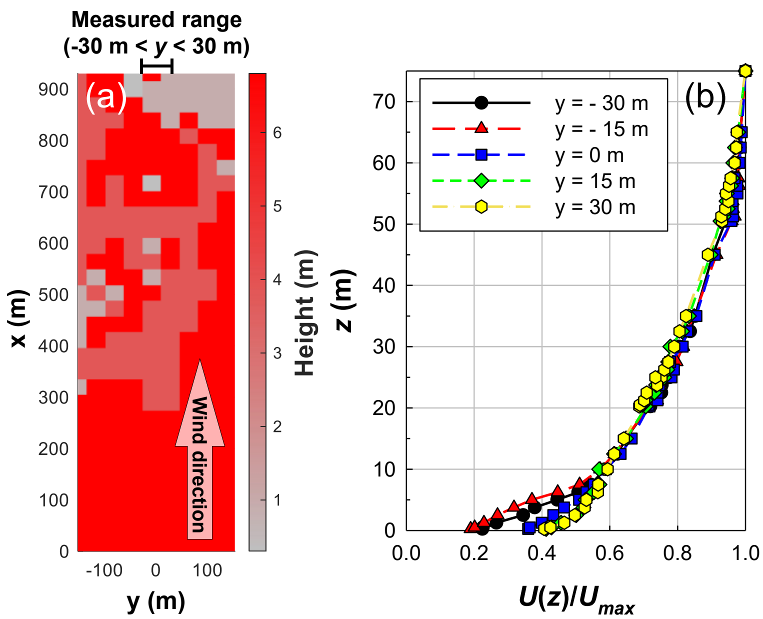

Fig. 10. Measured crosswind mean wind profiles at site 40 in a 1:50 scale: (a) Block height map; and (b) Measured mean wind profiles at different *y* locations.

4. Terrain Complexity and Wind Characteristics

4.1. Variations in Wind Characteristics Due to Complex Heterogeneous Terrain

Fig. 11 showcases semi-logarithmic profiles obtained from three wind tunnel testing results: one homogeneous terrain and two complex heterogeneous terrains. The logarithmic wind law model (Eq. (1)) is also included for reference. The $z_{0,eff}$ values for these terrains are all similar at full-scale, about 0.3 m. The $z_{0,eff}$ was determined through the calibration process outlined in Appendix B for the homogeneous terrain. For the heterogeneous terrains, the $z_{0,eff}$ was calculated using a grid-squared average-based approach, as discussed in Section 3.2. Given the established relationships between z_0 and other aerodynamic roughness parameters (d and u*) outlined in Appendix B, it was assumed that all terrains had similar d and u* values.

In Fig. 11, H and δ represent the block height and the gradient height of the homogeneous terrain, respectively. The gradient height was estimated using the method proposed by Caterelli et al. [53] based on the measured wind profile over the homogeneous terrain. The inertial sublayer (ISL) is typically observed between $H < z < 0.25\delta$, and the mean wind profile in this layer can be accurately described by Eq. (1) [15, 53]. Site 29 exhibits a consistent result with the theoretical solution and the homogeneous terrain within the ISL. However, site 33 deviates from the theoretical solution. Fig. 11 (b) demonstrates that site 33 features more pronounced terrain heterogeneity than site 29, indicating that even when $z_{0,eff}$ values are similar, the variations in wind profile can occur due to terrain heterogeneity. This discrepancy ultimately leads to errors when engineers estimate wind characteristics and loads. Therefore, it is crucial to quantify the differences between complex heterogeneous terrain and homogeneous terrain based on the degree of morphological complexity.

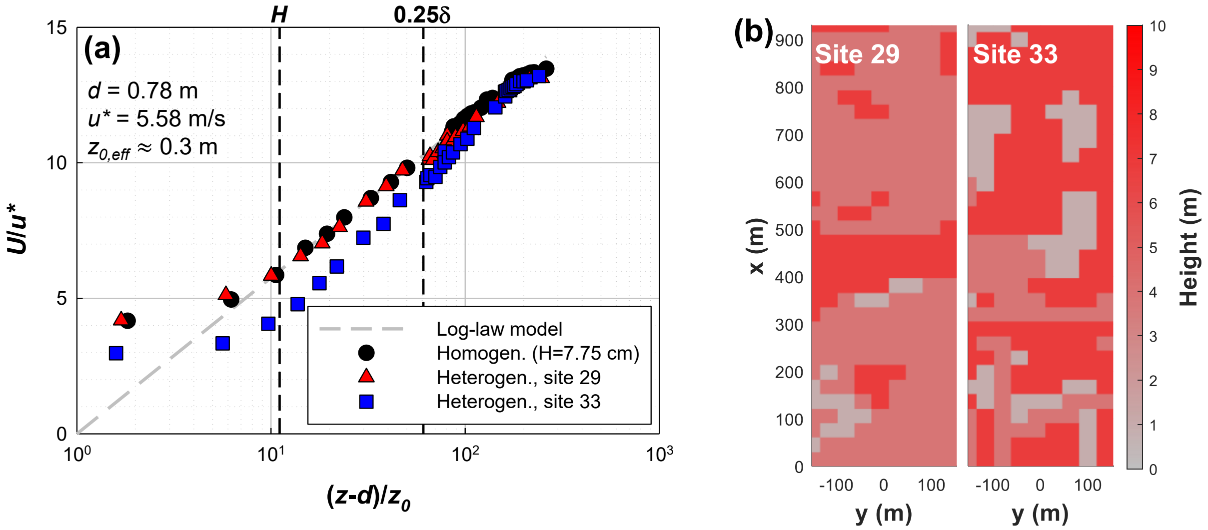

Fig. 11. Comparison of wind profiles over three different terrains with similar roughness length of 0.3 m in full-scale along with a theoretical model: (a) Semi-logarithmic wind profile; and (b) Block height maps for sites 29 and 33.

Fig. 12 provides a comparison of the normalized mean wind speed (U(10 m)/U_{max}), turbulence intensity (I_u(10 m)), and integral length scale (L_u(10 m)) between complex heterogeneous terrain and homogeneous terrain. The preliminary test regression analysis results for mean wind speed and turbulence intensity over homogeneous terrains are presented together (see Fig. B. 3 of Appendix B). Considerable dispersion were observed in the integral length scale, even on homogeneous terrain, represented by the scatter in the data. Over the heterogeneous terrain, both the mean wind speed and turbulence intensity exhibited similar trends but with greater variability. Moreover, relatively lower mean wind speeds and higher turbulence intensities were observed compared to the homogeneous terrains. The integral length scale in heterogeneous terrains showed larger magnitudes and greater variability. Notably, in areas where $z_{0,eff}$ was less than 0.1 m, the integral length scale reached up to 75 m on homogeneous terrain, while it exceeded 150 m on heterogeneous terrain. These findings demonstrate that the morphological complexity of the terrain introduces additional disturbances, resulting in lower mean wind speeds and higher turbulence intensities compared to homogeneous terrain.

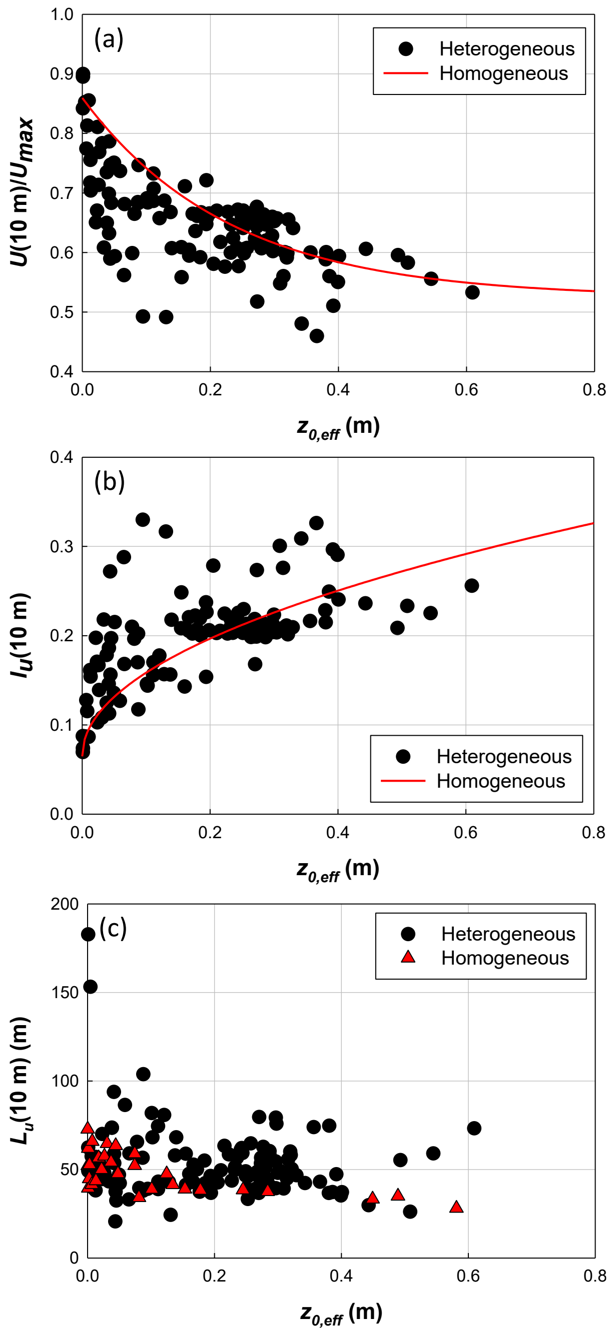

Fig. 12. Measured wind characteristics for heterogeneous and homogeneous terrains at a 10 m height: (a) Normalized mean wind speed; (b) Turbulence intensity; and (c) Integral length scale.

Fig. 13 shows the power spectrum of (a) homogeneous and (b) complex heterogeneous terrains at 10 m height, with similar $z_{0,eff}$ values. The Engineering Sciences Data Unit (ESDU) empirical model, described by Eq.(9) [54], is included in the plots for comparison.

$$\frac{nS_{uu}}{\sigma_u^2} = \frac{4f}{(1 + 70.8f^2)^{5/6}} \tag{9}$$

where n is the frequency in Hertz, S_{uu} is the power spectrum for the longitudinal turbulence component, σ_u is the standard deviation of the fluctuating wind components and $f = nL_u/U$ in which L_u is the longitudinal integral length scale and U is the longitudinal mean velocity. In high frequency, the power density of homogeneous terrain is larger than heterogeneous terrain. At $nL_u/U = 10$, the values of power density nS_{uu}/σ^2 are 0.042 and 0.038 for the homogeneous and heterogeneous terrains, respectively. It was confirmed that the heterogeneous terrain exhibits a rougher immediate upwind terrain compared to the homogeneous terrain, leading to enhanced energy dissipation and a smaller spectrum response.

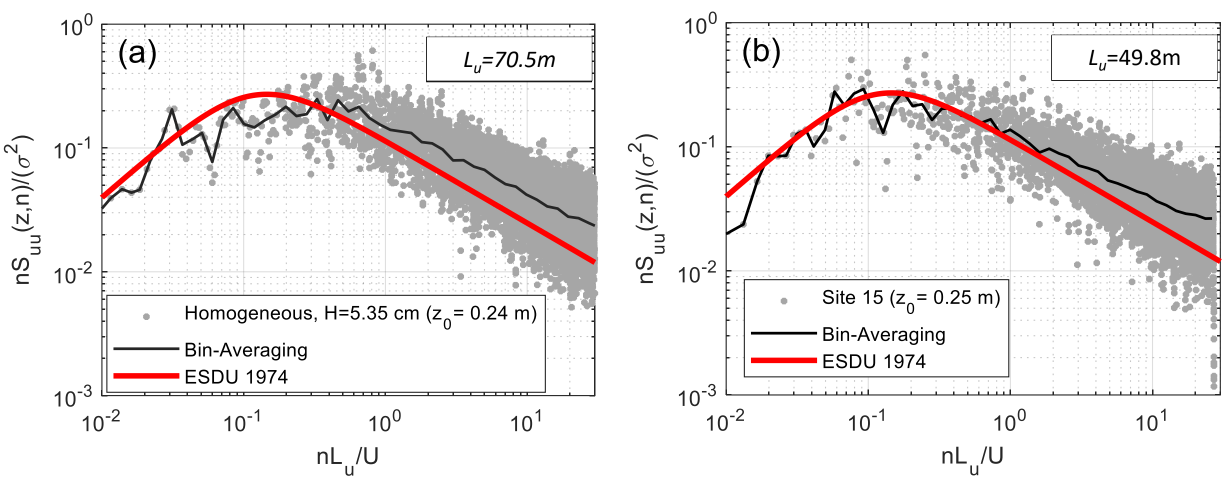

Fig. 13. Wind power spectrum at a 10 m height: (a) homogeneous terrain with $H = 5.35$ cm; and (b) heterogeneous terrain (site 15). Black curves represent the bin averages of the wind tunnel power spectrum.

4.2. Importance of Considering the Terrain Heterogeneity

To assess the impact of terrain complexity and understand the inaccuracies that arise when assuming a complex heterogeneous terrain as a homogeneous terrain, the difference in normalized mean wind speed ($\Delta_{U_{norm}}$) and turbulence intensity (Δ_{I_u}) between complex heterogeneous and homogeneous terrains was quantified using Eqs. (9) and (10):

$$\Delta_{U_{norm}}(z) = \frac{[U(z)/U_{max}]^{het.} - [U(z)/U_{max}]^{hom.}}{[U(z)/U_{max}]^{heterogen.}} \tag{10}$$

$$\Delta_{I_u}(z) = \frac{I_u^{het.}(z) - I_u^{hom.}(z)}{I_u^{het.}(z)} \tag{11}$$

Here, the superscripts $^{het.}$ and $^{hom.}$ represent values measured under heterogeneous and homogeneous conditions, respectively. The $[U(z)/U_{max}]^{hom.}$ and $I_u^{hom.}(z)$ denote the corresponding values obtained from the red line in Fig. 12, using the $z_{0,eff}$ value of the target heterogeneous site.

Fig. 14 presents $\Delta_{U_{norm}}$ and Δ_{I_u} at heights of 10 m and 30 m. The variations of $\Delta_{U_{norm}}$ and Δ_{I_u} are depicted based on changes in $z_{0,eff}$, categorized into ranges of $\mathrm{COV}_{ln(z_0)}$. The figure highlights the importance of considering heterogeneity even when a homogeneous assumption may appear acceptable. First, it was observed that the difference between heterogeneous and homogeneous terrains is significant for lower $z_{0,eff}$ values, indicating relatively smooth terrains. In these cases, the influence of terrain complexity on wind characteristics becomes more prominent. As $z_{0,eff}$ increases, a general trend of decreasing difference can be observed. Although the difference becomes smaller when $z_{0,eff}$ exceeds 0.4 m, further research is needed to investigate this range since the current study focused on $z_{0,eff}$ values below 0.4 m. Second, when $z_{0,eff}$ levels are similar, larger differences compared to the homogeneous terrain are observed for higher $\mathrm{COV}_{ln(z_0)}$ ranges. For instance, in the $z_{0,eff}$ range of 0.2 to 0.4, the normalized mean wind speed decreases by up to 10% in the $\mathrm{COV}_{ln(z_0)}$ range of 0.5 to 1.0, while it decreases by as much as 30% in the $\mathrm{COV}_{ln(z_0)}$ range of 1.0 to 1.5.

Fig. 14 (c) and (d) demonstrate that at a height of 30 m, the difference between homogeneous and heterogeneous terrains decreases compared to 10 m. Notably, $\Delta_{U_{norm}}$ shows a more substantial decrease compared to Δ_{I_u}. Although the magnitude of the mean wind speed difference decreased significantly to about -20% at 30 m, the turbulence intensity still exhibited variations of up to 50% compared to homogeneous terrains. It suggested that the flow disturbance caused by terrain complexity continues to affect the turbulent flow component at 30 m height. Since turbulence intensity directly influences flow separation and reattachment phenomena on the surface of structures, it is important to note the sustained higher difference in turbulence intensity when estimating wind loads.

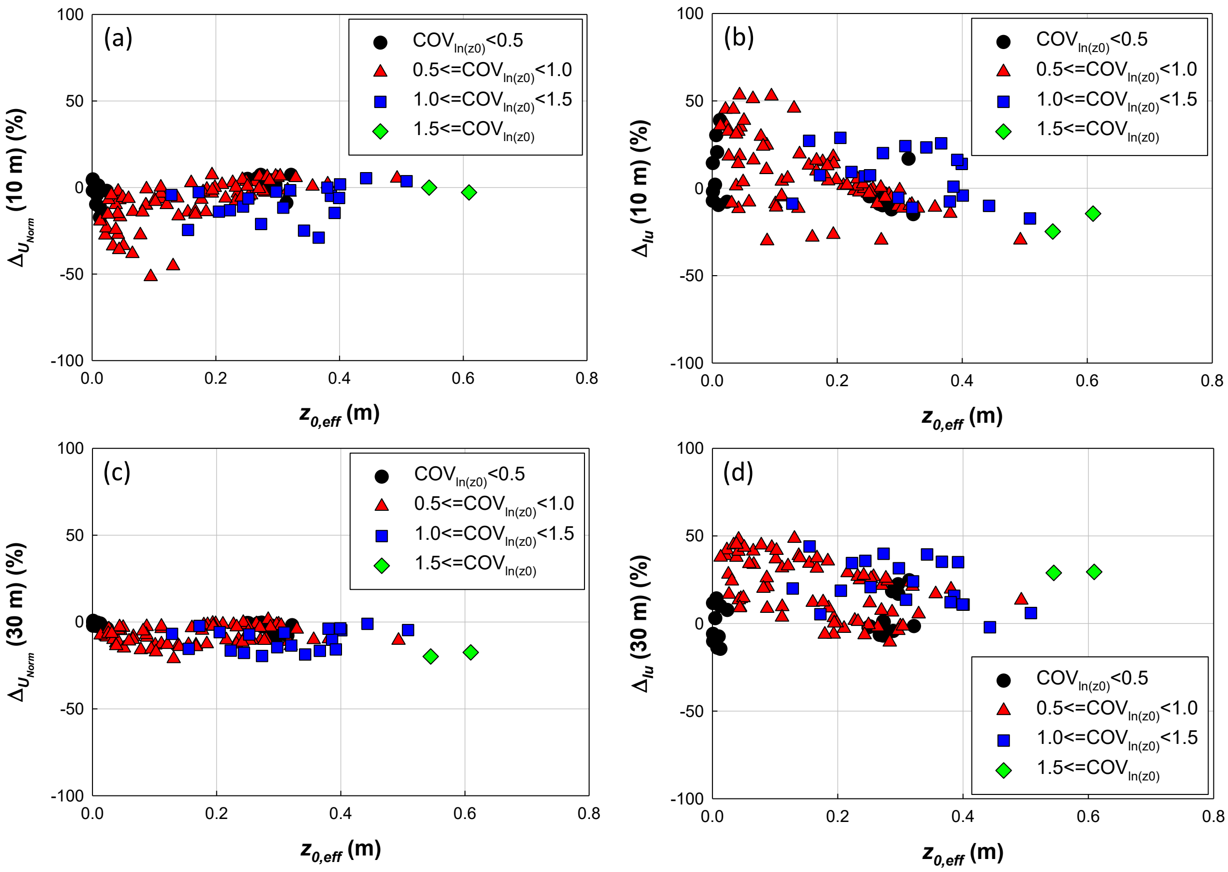

Fig. 14. Relationship between $z_{0,eff}$ and difference in wind characteristics between homogeneous and complex heterogeneous terrain.: (a) $\Delta_{U_{norm}}$ for 10 m height; (b) Δ_{I_u}.for 10 m height; (c) $\Delta_{U_{norm}}$ for 30 m height; and (d) Δ_{I_u}.for 30 m height.

4.3. Simplified Model to Estimate the Effect of Heterogeneous Terrain

In cases where the T_{COV} exceeds 0.25 and wind tunnel testing is not feasible, it may be valuable for engineers and researchers to approximate the impact of heterogeneous terrain. Next, we aimed to approximate the wind speed and turbulence intensity at 10 m and 30 m heights based on the morphological information of the terrain. To achieve this, we analyzed the trends observed in the $z_{0,eff}$-$\mathrm{COV}_{ln(z_0)}$-wind characteristics relationship, as shown in Fig. 15.

First, we observed that as $\mathrm{COV}_{ln(z_0)}$ increased, the mean wind speed decreased while the turbulence intensity increased. This relationship was found to be negatively linear for mean wind speed and positively linear for turbulence intensity, as indicated by the red area in the plot. These correlations held across a wide range of $z_{0,eff}$ values. Second, it was identified that the influence of $z_{0,eff}$ was the primary factor, with $\mathrm{COV}_{ln(z_0)}$ making a secondary contribution. For instance, in a homogeneous terrain with a $z_{0,eff}$ value of 0.2 m, the normalized mean wind speed was approximately 0.7 and the turbulence intensity was around 0.2, as shown in Fig. 12. In Fig. 15, even when the $\mathrm{COV}_{ln(z_0)}$ decreased, the normalized mean wind speed for the range of $z_{0,eff}$ 0.2-0.3 (represented by blue squares) did not exceed 0.7, and the turbulence intensity did not decrease below 0.2.

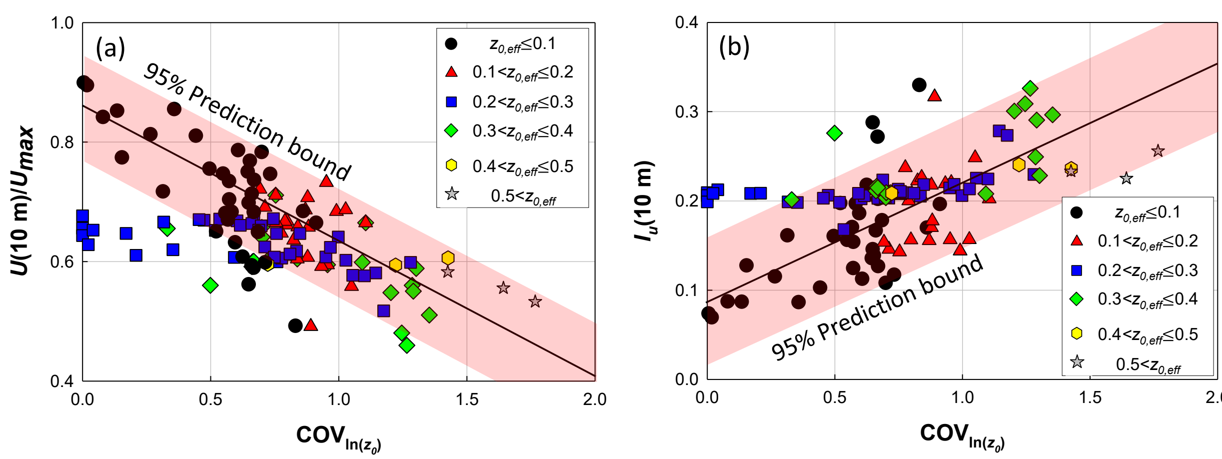

Fig. 15. Relationship between $\mathrm{COV}_{ln(z_0)}$ and wind characteristics: (a) Normalized mean wind speed at a 10 m height; and (b) Turbulence intensity at 10 m height.

The linear relationship corresponding to the first trend mentioned above was quantified through regression analysis, resulting in the derivation of Eqs. (12) to (15), which represent the relationships between $\mathrm{COV}_{ln(z_0)}$ and wind characteristics at 10 m and 30 m heights:

$$\frac{U(10\ m)}{U_{max}} = 0.86 - 0.23\mathrm{COV}_{ln(z_0)} \quad (12)$$

$$\frac{U(30\ m)}{U_{max}} = 0.92 - 0.12\mathrm{COV}_{ln(z_0)} \quad (13)$$

$$I_u\,(10\ m) = 0.09 + 0.13\mathrm{COV}_{ln(z_0)} \quad (14)$$

$$I_u\,(30\ m) = 0.06 + 0.07\mathrm{COV}_{ln(z_0)} \quad (15)$$

The simplified relationship between $z_{0,eff}$, $\mathrm{COV}_{ln(z_0)}$, and wind characteristics at 10 m height was depicted in Fig. 16 by combining the regression results for the first trend and the second trend.

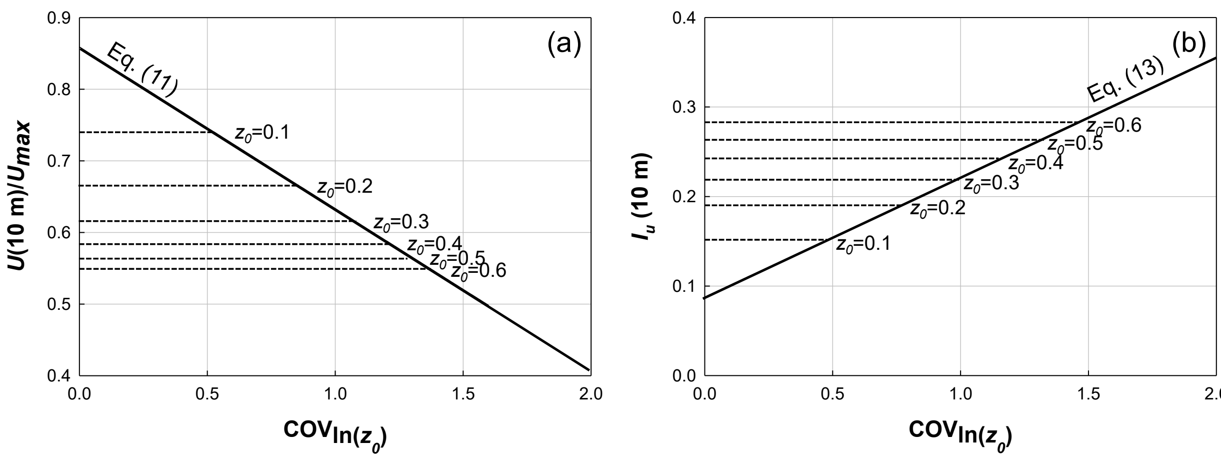

Fig. 16. Simplified model between $z_{0,eff}$-$\mathrm{COV}_{ln(z_0)}$-wind characteristics at a 10 m height: (a) Normalized mean wind speed; and (b) Turbulence intensity.

4.4. Effect of Terrain Transition Type

Thus far, we have analyzed the heterogeneous effect by considering the effective roughness length and morphological variation of the terrain. An additional important parameter to consider is the terrain transition type, which can be classified as rough-to-smooth (R-S) or smooth-to-rough (S-R).

Out of the 120 cases analyzed, the roughness change detection algorithm identified 54 cases where a roughness change was detected. Fig. 17 shows the relationship between the roughness change parameter $M = \ln\left(z_{0,eff}^{up}/z_{0,eff}^{down}\right)$, and the ratio of measured wind characteristics for complex heterogeneous and homogeneous terrains. The $z_{0,eff}$ value of the complex heterogeneous terrain was employed to select the corresponding homogeneous terrain results.

The S-R transition showed greater variability compared to the R-S transition when compared to the homogeneous terrain. This difference can be attributed to the time or distance required for the wind flow to reach equilibrium with the downstream terrain after the transition. According to Deaves [22], rough-to-smooth changes usually have a larger horizontal extent for the transition region compared to smooth-to-rough changes. Consequently, it takes a significant amount of time for the wind flow in the internal boundary layer to adjust to the downwind terrain in the case of an R-S change. On the other hand, the mean wind profile adapts more quickly during an S-R change [55-57]. The R-S transition requires a fetch length that is more than twice as long as the S-R transition to reach equilibrium [33]. As a result, the wind flow in the S-R change undergoes rapid modifications to achieve equilibrium with the downwind terrain, leading to a greater difference compared to a homogeneous terrain with a similar $z_{0,eff}$.

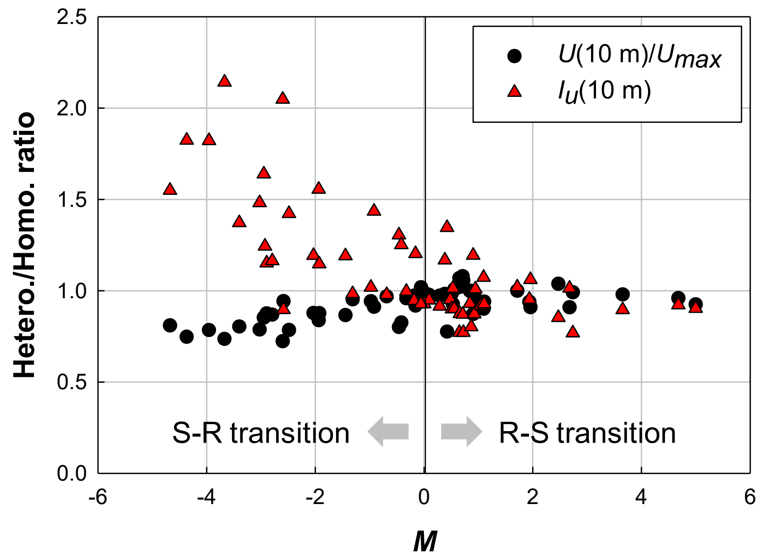

Fig. 17. Relationship between *M* and wind characteristics for cases where roughness changes occurred.

5. Conclusions

This study conducted extensive BLWT testing on complex heterogeneous terrain sites to investigate the impact of terrain complexity on near-surface wind profiles. The findings shed light on the importance of accurately characterizing terrain heterogeneity and considering roughness changes in wind profile and load assessments. The main findings are as follows:

- The developed prediction process showed promising performance in predicting mean wind speeds by considering the morphological information of complex heterogeneous terrain. The prediction error exhibited high accuracy, with an average of less than 2%. The process improved prediction performance by incorporating a mathematical change detection algorithm to quantitatively and automatically identify roughness changes compared to the equivalent homogeneous assumption. Further investigation revealed that an increase in $\mathrm{COV}_{ln(z_0)}$ had a detrimental impact on the prediction performance, even when $z_{0,eff}$ values were similar. However, the negative effect of $\mathrm{COV}_{ln(z_0)}$ on prediction performance diminished as $z_{0,eff}$ values increased.

- It was observed that assuming complex heterogeneous terrain as homogeneous terrain can result in significant differences of up to 50% in assessing wind characteristics. These differences were particularly pronounced for terrains with lower $z_{0,eff}$ values, indicating relatively smoother surfaces. This observation underscored the potential for significant reductions in mean wind speeds by considering terrain complexity, particularly for terrain classes classified as lower than the very rough category (z_0 = 0.5 m according to Davenport's roughness classification). Notably, the influence of terrain complexity on wind characteristics became negligible when $z_{0,eff}$ exceeds 0.5 m.

- A simplified model was developed to estimate the impact of heterogeneous terrain on wind characteristics. This model quantifies the relationship between $z_{0,eff}$-$\mathrm{COV}_{ln(z_0)}$-wind characteristics. Two important trends were observed in this relationship. First, as $\mathrm{COV}_{ln(z_0)}$ increased, the mean wind speed decreased while turbulence intensity increased. Second, the dominant factor influencing wind characteristics was $z_{0,eff}$, with a secondary contribution from $\mathrm{COV}_{ln(z_0)}$. Building upon these trends, a simplified relationship was proposed between $z_{0,eff}$, $\mathrm{COV}_{ln(z_0)}$, and wind characteristics, accompanied by corresponding equations. This model provided a tool for estimating wind characteristics roughly in complex heterogeneous terrains.

- In future studies, the impact of wind characteristics variation induced by complex heterogeneous terrains on building structures will be investigated through wind tunnel testing. The research aims to quantify the variability of the pressure coefficient that can arise in terrains with similar z_0 values. By conducting these experiments, a better understanding of the effects of terrain complexity on building performance can be gained.

Appendix A. Selected Sites

The coordinates of the selected 60 sites are presented in Table A. 1.

Table A. 1. Coordinates of selected sites and the wind direction.

Site ID	Latitude	Longitude	Direction from magnetic north	Site ID	Latitude	Longitude	Direction from magnetic north
1	30.68526	-88.0254	0	31	38.06936	-75.5499	90
2	27.6763	-97.2861	270	32	41.20402	-73.0934	90
3	43.18735	-77.6305	90	33	36.0522	-86.8092	270
4	30.41956	-84.318	0	34	34.44947	-77.5262	90
5	44.24718	-72.5886	90	35	41.38552	-71.494	180
6	41.7158	-73.9159	180	36	37.67902	-75.6308	90
7	38.06936	-75.5499	180	37	38.72918	-90.4551	90
8	33.67731	-79.0314	0	38	25.41191	-80.4964	270
9	30.22528	-92.0613	90	39	31.59068	-83.2424	0
10	41.02429	-73.6259	90	40	43.62806	-72.5149	270
11	31.06005	-81.4208	0	41	34.93197	-81.0286	270
12	33.89831	-78.4307	270	42	40.76147	-73.4698	0
13	38.45491	-75.058	90	43	37.79596	-80.2998	180
14	42.87553	-71.9509	270	44	40.6656	-73.9868	90
15	36.76553	-76.3582	90	45	30.2068	-93.2414	180
16	30.4202	-81.5567	90	46	37.6916	-75.7141	0
17	38.20711	-75.6946	0	47	39.05953	-84.6102	90
18	35.67342	-105.911	90	48	38.72754	-75.2634	0
19	39.90773	-75.1917	0	49	30.28072	-87.5809	270
20	31.20489	-85.4051	180	50	44.32527	-69.7537	0
21	30.50375	-89.6601	270	51	39.3208	-74.5953	60
22	39.8525	-88.906	0	52	28.1937	80.6056	200
23	30.26644	-89.415	0	53	26.3304	81.7791	250
24	34.81752	-82.4157	180	54	29.5385	89.7751	170
25	36.75083	-96.0075	270	55	29.5385	-89.7751	25
26	41.33751	-71.7566	180	56	35.2322	-75.6215	35
27	37.73784	-88.946	90	57	35.2322	-75.6215	80
28	37.96214	-91.7524	0	58	35.2322	-75.6215	155
29	31.07034	-81.4076	180	59	35.2322	-75.6215	80
30	32.9042	-79.9706	0	60	28.6119	-96.6252	80

Appendix B. Preliminary Wind Tunnel Tests on Homogeneous Terrains

Preliminary wind tunnel tests were performed on homogeneous terrains. The block height was varied from 6.5 mm to 160 mm, and mean wind profiles were measured to extract Aerodynamic Roughness Parameters (ARPs) corresponding to different block heights (H). The calibration procedure for ARPs is detailed in Catarelli et al. [53]. Fig. B. 1 illustrates the relationship between H and z_0 in the test scale, where z_0 increases with increasing H. By multiplying the length scales, the z_0 values can be transformed to full-scale z_0. Additionally, Fig. B. 2 depicts the relationships between z_0 and other ARPs (u_* and d), which were utilized to determine the ARPs for the D.H. model.

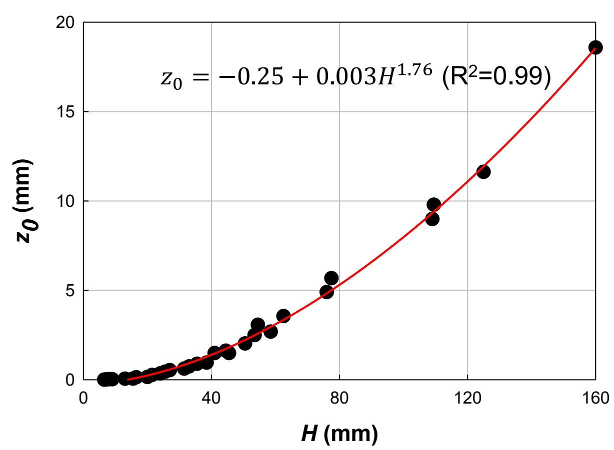

Fig. B. 1. Relationship between H and z_0 in test scale for homogeneous terrain.

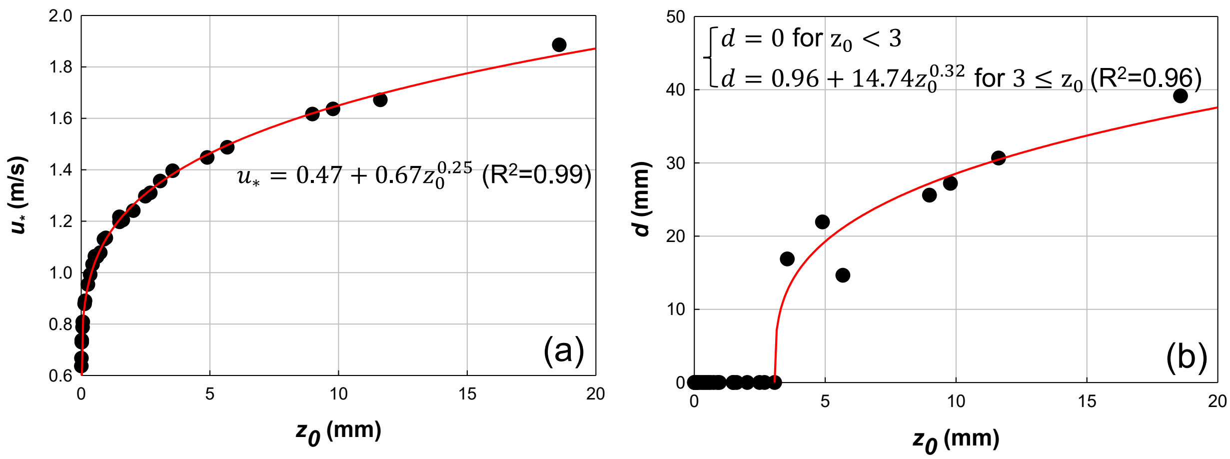

Fig. B. 2. Relationship between z_0 and other ARPs in test scale for homogeneous terrain: (a) u_*; and (b) d.

Fig. B. 3 presents the normalized mean wind speed and turbulence intensity as a function of z_0. It showed a general trend where the mean wind speed decreases and the turbulence intensity increases with increasing z_0. Regression analysis was conducted to establish relationships between z_0 and wind characteristics in a homogeneous terrain.

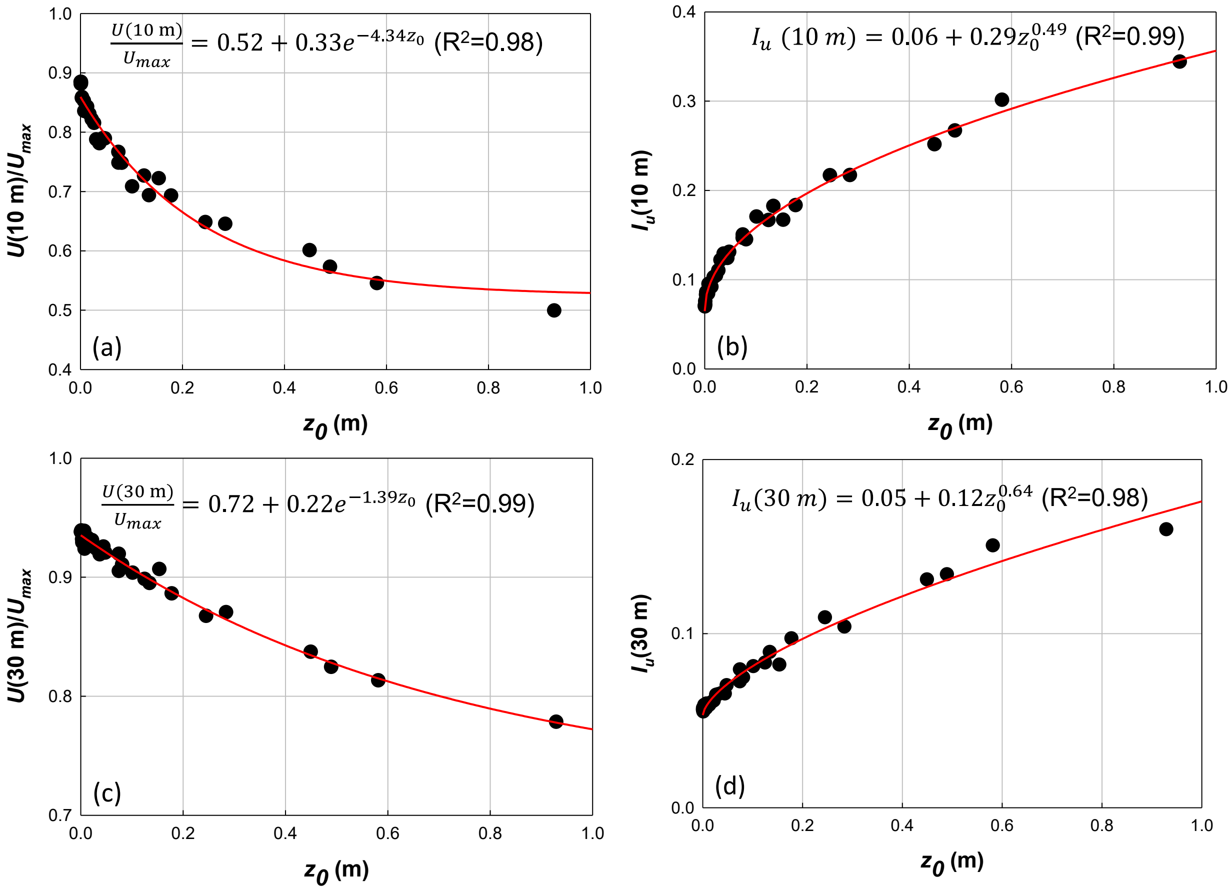

Fig. B. 3. Relationship between z_0 and wind characteristics at 10 m-height in full scale for homogeneous terrains: (a) normalized mean wind speed at 10 m height; (b) turbulence intensity at 10 m height; (c) normalized mean wind speed at 30 m height; and (d) turbulence intensity at 30 m height.

Acknowledgments

This material is based upon work supported by the National Science Foundation under Grant No. CMMI-1856205. Any opinions, findings, and conclusions or recommendations expressed in this material are those of the authors and do not necessarily reflect the views of the National Science Foundation.

References

[1] E.F. Bradley, A micrometeorological study of velocity profiles and surface drag in the region modified by a change in surface roughness, Q. J. R. Meteorol. 94(401) (1968) 361-379. https://doi.org/10.1002/qj.49709440111.
[2] E.C. Choi, Field measurement and experimental study of wind speed profile during thunderstorms, J. Wind. Eng. Ind. Aerod. 92(3-4) (2004) 275-290. https://doi.org/10.1016/j.jweia.2003.12.001.
[3] N. Antoniou, H. Montazeri, M. Neophytou, B. Blocken, CFD simulation of urban microclimate: Validation using high-resolution field measurements, Sci. Total Environ. 695 (2019) 133743. https://doi.org/10.1016/j.scitotenv.2019.133743.
[4] Y. Tamura, K. Suda, A. Sasaki, K. Miyashita, Y. Iwatani, T. Maruyama, K. Hibi, R. Ishibashi, Simultaneous wind measurements over two sites using Doppler sodars, J. Wind. Eng. Ind. Aerod. 89(14-15) (2001) 1647-1656. https://doi.org/10.1016/S0167-6105(01)00149-0.
[5] J. Counihan, An improved method of simulating an atmospheric boundary layer in a wind tunnel, Atmospheric Environment (1967) 3(2) (1969) 197-214. https://doi.org/10.1016/0004-6981(69)90008-0.
[6] J. Counihan, Simulation of an adiabatic urban boundary layer in a wind tunnel, Atmospheric Environment (1967) 7(7) (1973) 673-689. https://doi.org/10.1016/0004-6981(73)90150-9.
[7] N. Cook, On simulating the lower third of the urban adiabatic boundary layer in a wind tunnel, Atmospheric Environment (1967) 7(7) (1973) 691-705. https://doi.org/10.1016/0004-6981(73)90151-0.
[8] N. Cook, Determination of the model scale factor in wind-tunnel simulations of the adiabatic atmospheric boundary layer, J. Wind. Eng. Ind. Aerod. 2(4) (1978) 311-321. https://doi.org/10.1016/0167-6105(78)90016-8.
[9] H. Irwin, The design of spires for wind simulation, J. Wind. Eng. Ind. Aerod. 7(3) (1981) 361-366. https://doi.org/10.1016/0167-6105(81)90058-1.
[10] H. Kozmar, Scale effects in wind tunnel modeling of an urban atmospheric boundary layer, Theor. Appl. Climatol. 100 (2010) 153-162. https://doi.org/10.1007/s00704-009-0156-3.
[11] H. Kozmar, Truncated vortex generators for part-depth wind-tunnel simulations of the atmospheric boundary layer flow, J. Wind. Eng. Ind. Aerod. 99(2-3) (2011) 130-136. https://doi.org/10.1016/j.jweia.2010.11.001.
[12] J. Yu, M. Li, T. Stathopoulos, Q. Zhou, X. Yu, Urban exposure upstream fetch and its influence on the formulation of wind load provisions, Build. Environ. 203 (2021) 108072. https://doi.org/10.1016/j.buildenv.2021.108072.
[13] S. Jung, F. Masters, Characterization of open and suburban boundary layer wind turbulence in 2008 Hurricane Ike, Wind and structures 17(2) (2013) 135-162. http://dx.doi.org/10.12989/was.2013.17.2.135
[14] C. Grimmond, T.R. Oke, Aerodynamic properties of urban areas derived from analysis of surface form, J. Appl. Meteorol. Climatol. 38(9) (1999) 1262-1292. https://doi.org/10.1175/1520-0450(1999)038%3C1262:APOUAD%3E2.0.CO;2.
[15] J. Wiernga, Representative roughness parameters for homogeneous terrain, Bound. Layer Meteorol. 63(4) (1993) 323-363. https://doi.org/10.1007/BF00705357.
[16] A.K. Blackadar, The vertical distribution of wind and turbulent exchange in a neutral atmosphere, J. Geophys. Res. 67(8) (1962) 3095-3102. https://doi.org/10.1029/JZ067i008p03095.
[17] H. Schmid, B. Bünzli, The influence of surface texture on the effective roughness length, Q. J. R. Meteorol. 121(521) (1995) 1-21. https://doi.org/10.1002/qj.49712152102.

[18] H.A. Panofsky, A. Townsend, Change of terrain roughness and the wind profile, Q. J. R. Meteorol. 90(384) (1964) 147-155. https://doi.org/10.1002/qj.49709038404.
[19] A. Townsend, The response of a turbulent boundary layer to abrupt changes in surface conditions, J. Fluid Mech. 22(4) (1965) 799-822. https://doi.org/10.1017/S0022112065001155.
[20] N.S. Ghaisas, A predictive analytical model for surface shear stresses and velocity profiles behind a surface roughness jump, Bound. Layer Meteorol. 176(3) (2020) 349-368. https://doi.org/10.1007/s10546-020-00535-8.
[21] D.M. Deaves, R.I. Harris, A mathematical model of the structure of strong winds, CIRIA Report 76, Const Ind. Research and Inf. Assoc. (1978).
[22] D. Deaves, Computations of wind flow over changes in surface roughness, J. Wind. Eng. Ind. Aerod. 7(1) (1981) 65-94. https://doi.org/10.1016/0167-6105(81)90068-4.
[23] N.J. Cook, The Deaves and Harris ABL model applied to heterogeneous terrain, J. Wind. Eng. Ind. Aerod. 66(3) (1997) 197-214. https://doi.org/10.1016/S0167-6105(97)00034-2.
[24] C.W. Kent, C.S.B. Grimmond, D. Gatey, J.F. Barlow, Assessing methods to extrapolate the vertical wind-speed profile from surface observations in a city centre during strong winds, J. Wind. Eng. Ind. Aerod. 173 (2018) 100-111. https://doi.org/10.1016/j.jweia.2017.09.007.
[25] K. Wang, T. Stathopoulos, Exposure model for wind loading of buildings, J. Wind. Eng. Ind. Aerod. 95(9-11) (2007) 1511-1525. https://doi.org/10.1016/j.jweia.2007.02.016.
[26] ASCE, Minimum design loads and associated criteria for buildings and other structures, American Society of Civil Engineers, 2017. https://doi.org/10.1061/9780784414248.
[27] BS, BS6399 Loading for Buildings. Part 2. Code of Practice for Wind Loads, British Standards Institution, London, 1995.
[28] ESDU, Data Item 82026. Strong winds in the atmospheric boundary layer. Part 1: hourly-mean wind speeds., Engineering Sciences Data Unit, 1993.
[29] R. Hanson, B. Ganapathisubramani, Development of turbulent boundary layers past a step change in wall roughness, J. Fluid Mech. 795 (2016) 494-523. https://doi.org/10.1017/jfm.2016.213.
[30] U. Ismail, T.A. Zaki, P.A. Durbin, Simulations of rib-roughened rough-to-smooth turbulent channel flows, J. Fluid Mech. 843 (2018) 419-449. https://doi.org/10.1017/jfm.2018.119.
[31] W. Li, C.-H. Liu, On the flow response to an abrupt change in surface roughness, Flow Turbul. Combust.. (2022) 1-23. https://doi.org/10.1007/s10494-021-00281-y.
[32] J.H. Lee, Turbulent boundary layer flow with a step change from smooth to rough surface, Int. J. Heat Fluid Flow 54 (2015) 39-54. https://doi.org/10.1016/j.ijheatfluidflow.2015.05.001.
[33] A. Rouhi, D. Chung, N. Hutchins, Direct numerical simulation of open-channel flow over smooth-to-rough and rough-to-smooth step changes, J. Fluid Mech. 866 (2019) 450-486. https://doi.org/10.1017/jfm.2019.84.
[34] B.L. Sill, C. Fang, Effect of upstream roughness element distribution on wind loads on low rise structures, J. Wind. Eng. Ind. Aerod. 36 (1990) 1289-1297. https://doi.org/10.1016/0167-6105(90)90125-V.
[35] H.-C. Lim, K. Tsukamoto, M. Ohba, K. Mizutani, Study on the surface pressure distribution of cubes in cross-wind arrays, J. Wind. Eng. Ind. Aerod. 133 (2014) 18-26. https://doi.org/10.1016/j.jweia.2014.07.009.
[36] J. Yu, Contribution to the Exposure Assessment for the Evaluation of Wind Effects on Buildings, Concordia University, 2022.
[37] N. Antoniou, H. Montazeri, H. Wigo, M.K.-A. Neophytou, B. Blocken, M. Sandberg, CFD and wind-tunnel analysis of outdoor ventilation in a real compact heterogeneous urban area:

Evaluation using "air delay", Build. Environ. 126 (2017) 355-372. https://doi.org/10.1016/j.buildenv.2017.10.013.
[38] F.J. Masters, Boundary Layer Wind Tunnel, Basic Operations Manual, University of Florida, Gainesville, FL, 2017.
[39] J. Liao, A.J. Hewitt, P. Wang, X. Luo, Y. Zang, Z. Zhou, Y. Lan, C. O'Donnell, Development of droplet characteristics prediction models for air induction nozzles based on wind tunnel tests, Int. J. Agric. Biol. Eng. 12(6) (2019) 1-6. 10.25165/j.ijabe.20191206.5014.
[40] T. Stathopoulos, Wind loads on low-rise buildings: a review of the state of the art, Eng. Struct. 6(2) (1984) 119-135. https://doi.org/10.1016/0141-0296(84)90005-1.
[41] C. Homer, J. Dewitz, L. Yang, S. Jin, P. Danielson, G. Xian, J. Coulston, N. Herold, J. Wickham, K. Megown, Completion of the 2011 National Land Cover Database for the conterminous United States–representing a decade of land cover change information, Photogramm. Eng. Remote Sens. 81(5) (2015) 345-354. https://doi.org/10.14358/PERS.81.5.345.
[42] R. Macdonald, R. Griffiths, D. Hall, An improved method for the estimation of surface roughness of obstacle arrays, Atmos. Environ. 32(11) (1998) 1857-1864. https://doi.org/10.1016/S1352-2310(97)00403-2.
[43] D. Arthur, S. Vassilvitskii, K-means++ the advantages of careful seeding, Proceedings of the eighteenth annual ACM-SIAM symposium on Discrete algorithms, 2007, pp. 1027-1035.
[44] A.G. Davenport, Rationale for determining design wind velocities, J. Struct. Div. 86(5) (1960) 39-68. https://doi.org/10.1061/JSDEAG.0000521.
[45] T. Vihma, H. Savijärvi, On the effective roughness length for heterogeneous terrain, Q. J. R. Meteorol. 117(498) (1991) 399-407. https://doi.org/10.1002/qj.49711749808.
[46] Y. He, P. Chan, Q. Li, Estimation of roughness length at Hong Kong International Airport via different micrometeorological methods, J. Wind. Eng. Ind. Aerod. 171 (2017) 121-136. https://doi.org/10.1016/j.jweia.2017.09.019.
[47] J.C. Kaimal, J.J. Finnigan, Atmospheric boundary layer flows: their structure and measurement, Oxford university press1994.
[48] A.K. Blackadar, H. Tennekes, Asymptotic similarity in neutral barotropic planetary boundary layers, J. Atmos. Sci. 25(6) (1968) 1015-1020. https://doi.org/10.1175/1520-0469(1968)025%3C1015:ASINBP%3E2.0.CO;2.
[49] N.J. Cook, Designers guide to wind loading of building structures. Part 1, (1986).
[50] H. Schlichting, K. Gersten, Boundary-layer theory, springer2016.
[51] R. Killick, P. Fearnhead, I.A. Eckley, Optimal detection of changepoints with a linear computational cost, J. Am. Stat. Assoc. 107(500) (2012) 1590-1598. https://doi.org/10.1080/01621459.2012.737745.
[52] P.A. Taylor, Comments and further analysis on effective roughness lengths for use in numerical three-dimensional models, Bound. Layer Meteorol. 39(4) (1987) 403-418. https://doi.org/10.1007/BF00125144.
[53] R. Catarelli, P. Fernández-Cabán, F. Masters, J. Bridge, K. Gurley, C. Matyas, Automated terrain generation for precise atmospheric boundary layer simulation in the wind tunnel, J. Wind. Eng. Ind. Aerod. 207 (2020) 104276. https://doi.org/10.1016/j.jweia.2020.104276.
[54] ESDU, Characteristics of atmospheric turbulence near the ground, Part I: Definitions and general information, Engineering Sciences Data Unit 74030 (1974).
[55] H. Panofsky, D. Larko, R. Lipschut, G. Stone, E. Bradley, A.J. Bowen, J. Højstrup, Spectra of velocity components over complex terrain, Q. J. R. Meteorol. 108(455) (1982) 215-230. https://doi.org/10.1002/qj.49710845513.

[56] A. Beljaars, P. Schotanus, F. Nieuwstadt, Surface layer similarity under nonuniform fetch conditions, J. Appl. Meteorol. Climatol. (1983) 1800-1810. https://doi.org/10.1175/1520-0450(1983)022%3C1800:SLSUNF%3E2.0.CO;2.
[57] H.W. Tieleman, Wind tunnel simulation of wind loading on low-rise structures: a review, J. Wind. Eng. Ind. Aerod. 91(12-15) (2003) 1627-1649. https://doi.org/10.1016/j.jweia.2003.09.021.